Research on Chemical Intermediates
https://doi.org/10.1007/s11164-019-03860-x

Magnetic calcined oyster shell functionalized with taurine immobilized on β-cyclodextrin (Fe_3O_4/COS@β-CD-SO_3H NPs) as green and magnetically reusable nanocatalyst for efficient and rapid synthesis of spirooxindoles

Narges Mohammadian[1] · **Batool Akhlaghinia**[1]

Received: 17 February 2019 / Accepted: 15 May 2019

Abstract

Magnetic calcined oyster shell functionalized with taurine immobilized on β-cyclodextrin (Fe_3O_4/COS@β-CD-SO_3H NPs) was prepared as a new stable, long-lived, highly efficient, and exceptional reusable magnetic nanostructured catalyst. The as-prepared solid acidic catalyst was characterized by various spectroscopic and microscopic techniques such as Fourier-transform infrared (FT-IR) spectroscopy, X-ray diffraction (XRD) analysis, scanning electron microscopy (SEM), energy-dispersive X-ray (EDX) spectroscopy, transmission electron microscopy (TEM), vibrating-sample magnetometry (VSM), thermogravimetric analysis (TGA)/differential thermogravimetry (DTG), and elemental (CHNS) analysis. The results clearly showed that the synthesized superparamagnetic catalyst existed as uniform spheres with average particle size of 16–25 nm. The new magnetic nanocatalyst (Fe_3O_4/COS@β-CD-SO_3H NPs) was found to be very effective in one-pot multi-component reaction of isatin, active methylene component, and 1,3-dicarbonyl compounds for rapid preparation of spirooxindoles with fused chromenes in water in excellent yield. The most promising features of the presented approach are the short reaction time (15–22 min), magnetic separation of the nanostructured catalyst, simple work-up procedure, reusability of the catalyst for at least eight successive runs without any appreciable loss of activity, and high product yields (about 94–98%). Surprisingly,

Electronic supplementary material The online version of this article (https://doi.org/10.1007/s11164-019-03860-x) contains supplementary material, which is available to authorized users.

✉ Batool Akhlaghinia
akhlaghinia@um.ac.ir

[1] Department of Chemistry, Faculty of Science, Ferdowsi University of Mashhad, Mashhad 9177948974, Iran

Published online: 25 May 2019

the present methodology proved to be environmentally sustainable, low cost, and industrially profitable for scale-up and commercialization.

Graphical abstract A novel and green approach for synthesis of spirooxindoles using a green, inexpensive, and efficient nanocatalyst was investigated.

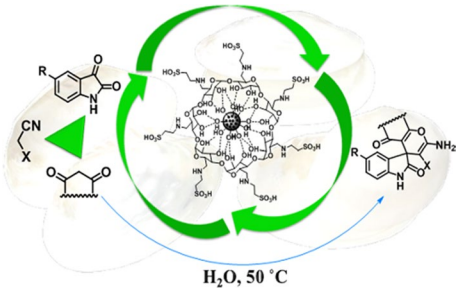

Keywords Spirooxindoles · Nanocatalyst · Taurine · Fe_3O_4 /COS@β-CD-SO_3H NPs

Introduction

Among *N*-heterocycle skeletons, the indole nucleus as a ''privileged scaffold'' is probably the most ubiquitous heterocyclic moiety, being found in a large variety of natural products and pharmaceuticals [1, 2]. Nitrile-substituted 4*H*-chromenes in particular have immense importance as effective drugs in human neurodegenerative disorders [3]. Several effective attempts to construct fused spirooxindoles via one-pot multicomponent reaction of isatin, active methylene component, and 1,3-dicarbonyl compounds are described in literature [4]. This type of reaction has been achieved using a number of different catalysts and conditions, such as triethylbenzylammonium chloride (TEBA) [5], Et_3N [6], I_2 [7], tetrabutylammonium fluoride (TBAF) [8], NH_4Cl [9], lipase [10], oxalic acid dihydrate:proline (LTTM) [11], ZnS nanoparticles [12], sodium stearate [13], butylmethylimidazolium tetrafluoroborate ([BMIm]BF_4) [14], SiO_2-OSO_3H NPs [15], amino-functionalized SBA-15 [16], $Cu(OAc)_2{\cdot}H_2O$ [17], ZrO_2 nanoparticles [18], nanocrystalline MgO [19], gluconic acid [20], $Mn(bpyo)_2$/MCM-41 [21], $MnFe_2O_4$ nanoparticles [22], silica sulfuric acid magnetic nanoparticle (SSA-MNPsd) [23], *S*-alkyl *O*-hydrogen sulfothioate-functionalized silica-coated magnetic nanoparticles (AHST-MNPs) [24], silica-bonded 5-*n*-propyl-octahydro-pyrimido[1,2-*a*]azepinium chloride (SB-DBU) Cl [25], carbon-SO_3H [26], ethylenediammonium diformate (EDDF) [27], and sulfated choline-based heteropolyanion [28].

While all reported approaches have their own merits, most of them are associated with one or more drawbacks such as use of carcinogenic organic solvents, application of high temperatures, harsh reaction conditions, poor yield, use of expensive and toxic catalysts, lack of catalyst reusability, consumption of large amounts of catalyst, and prolonged reaction time. Therefore, owing to the pharmaceutical

importance of spirooxindoles, development of new catalytic systems to overcome these shortcomings and enable simple, mild, green, and economical synthesis of spirooxindole derivatives remains important.

Based on the above discussion and our continuing efforts to develop novel and environmentally benign synthetic methodologies [29–59], we were prompted to design magnetic calcined oyster shell functionalized with taurine immobilized on β-cyclodextrin (Fe_3O_4/COS@β-CD-SO_3H NPs) to catalyze one-pot three-component synthesis of spirooxindoles with fused chromenes in water with excellent yield (Scheme 1).

Nowadays, magnetic nanoparticles (MNPs) have acquired immense importance in organic synthesis due to their unique properties such as high surface area, low toxicity, superparamagnetic behavior, high degree of chemical stability in various solvents, easy synthesis and modification, cost-effectiveness, and biocompatibility [60–63]. In particular, appropriate removal and recycling of Fe_3O_4 nanoparticles using an external magnet provides a separation method which is not time-consuming in comparison with standard methods (filtration and centrifugation), prevents loss of the heterogeneous catalyst during the separation process, and subsequently increases the purity of the products, as well as optimizing operational costs [64]. To improve the chemical stability and also prevent direct contact between magnetic nanoparticles, their surface has been coated by various materials such as titania [32], chitin [43], carbon [65, 66], polymer [67, 68], and hydroxyapatite [40]. The resultant nanocomposites with abundant hydroxyl groups (Fe_3O_4) on their surface can be efficiently functionalized using various function molecules for many special applications. Use of such functionalized magnetic nanocomposites or organocatalysts immobilized on coated iron oxide nanoparticles has been described for a number of organic transformations in literature [69–72]. Due to our interest in the development of new, efficient, and environmentally friendly catalysts [29–59], in the present study, synthesis and characterization of magnetic calcined oyster shell functionalized with taurine immobilized on β-cyclodextrin (Fe_3O_4/COS@β-CD-SO_3H NPs) were carried out and reported for the first time. Initially, calcined oyster shell nanoparticles (COS NPs) were generated by calcination of waste oyster shells at high temperature (900 °C for 6 h). Then, COS NPs (**I**) were magnetized by reaction between Fe^{2+} and Fe^{3+} ions and NH_4OH in presence of COS NPs (**I**). Afterwards,

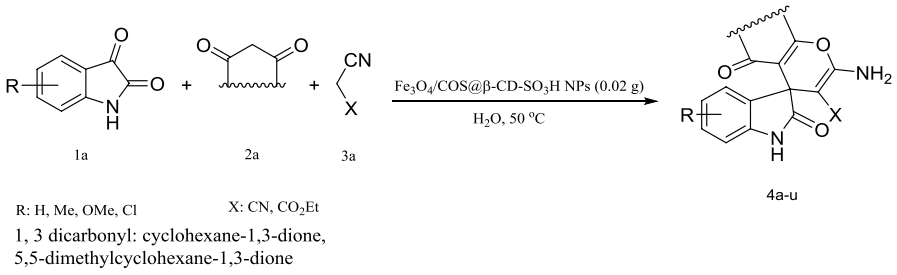

Scheme 1 Synthesis of different structurally spirooxindoles in presence of Fe_3O_4/CaO@β-CD-SO_3H NPs (**V**)

in continuation of our previous research on use of solid acids in organic synthesis [34, 38, 42, 46–52], preparation of Fe_3O_4/COS@β-CD-SO_3H NPs (**V**) as a new catalyst was investigated through functionalization of Fe_3O_4/COS NPs (**II**) by tosylated β-cyclodextrin (**III**) then immobilization of taurine (2-aminoethanesulfonic acid) on the surface of Fe_3O_4/COS@β-CDOTs (**IV**) (Scheme 2).

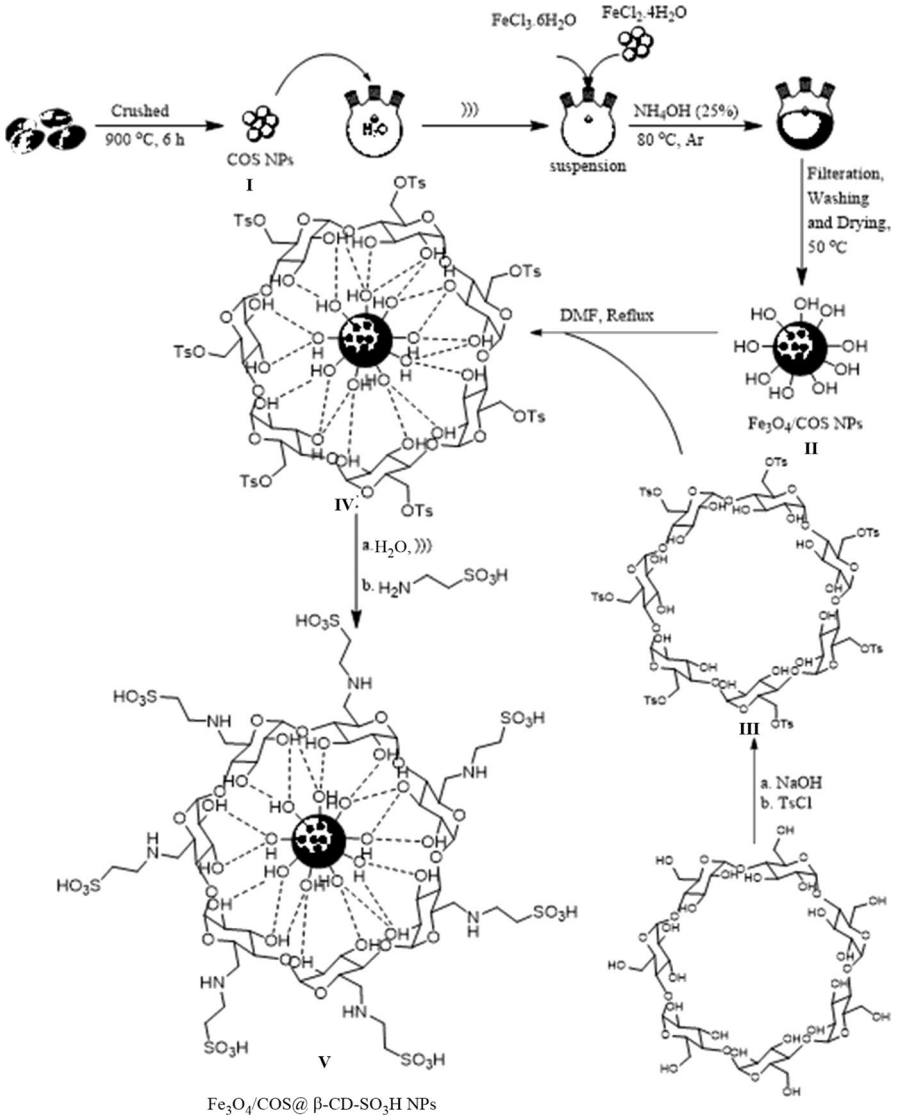

Scheme 2 Preparation of magnetic calcined oyster shell functionalized with taurine immobilized on β-cyclodextrin (Fe_3O_4/COS@β-CD-SO_3H NPs, **V**)

Results and discussion

Characterization of catalyst

Fe_3O_4/COS@β-CD-SO_3H NPs (**V**) as a magnetically reusable nanocatalyst was synthesized via the stepwise procedure illustrated in Scheme 2. Full characterization of this newly synthesized nanocatalyst was performed by Fourier-transform infrared (FT-IR) spectroscopy, X-ray powder diffraction (XRD) analysis, scanning electron microscopy (SEM), energy-dispersive X-ray (EDX) spectroscopy, transmission electron microscopy (TEM), vibrating-sample magnetometry (VSM), thermogravimetric analysis/differential thermogravimetry (TGA/DTG), and elemental (CHNS) analysis.

To confirm successful functionalization of Fe_3O_4/COS NPs (**II**) with β-CDOTs and then taurine, COS NPs (**I**), Fe_3O_4/COS NPs (**II**), β-CDOTs (**III**), Fe_3O_4/COS@β-CDOTs NPs (**IV**), and Fe_3O_4/COS@β-CD-SO_3H NPs (**V**) were characterized by FT-IR spectroscopy (Fig. 1). Figure 1a displays the FT-IR spectrum of COS NPs (**I**). The absorption band at around 1620–1332 cm^{-1} corresponds to stretching vibration of Ca–O bond, corroborating the presence of CaO phase in the structure of COS NPs. As seen in Fig. 1b, the significant new band at around 580 cm^{-1} is assigned to stretching vibration of Fe–O bond, illustrating successful bonding of Fe_3O_4 NPs to COS NPs (**I**) [73]. Broad stretching vibrations of OH groups were detected at around 3600–3000 cm^{-1}, related to absorptions by β-CD, –SO_3H, and Fe_3O_4. Also, the absorption band ranging from 2950 to 2780 cm^{-1} can be attributed to symmetric stretching of CH (Fig. 1c–f) [74, 75].

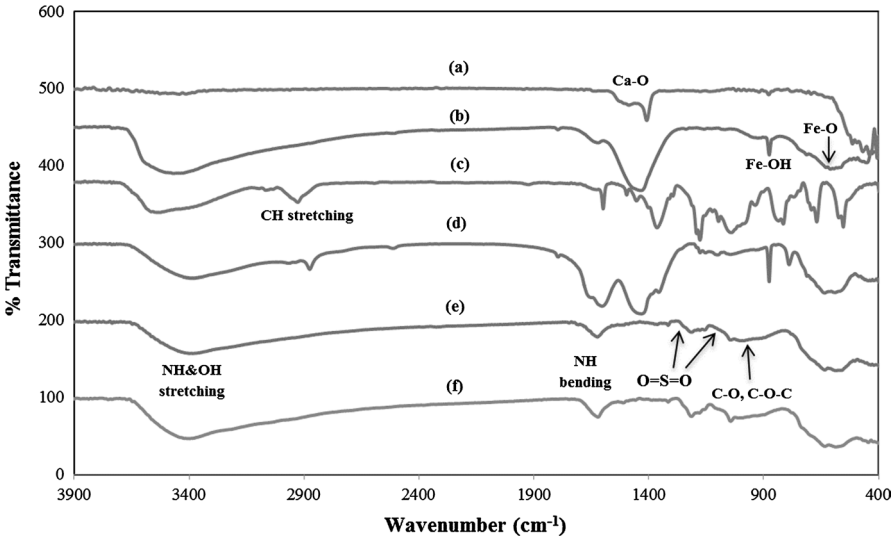

Fig. 1 FT-IR spectra of (a) COS NPs (**I**), (b) Fe_3O_4/COS NPs (**II**), (c) β-CDOTs (**III**), (d) Fe_3O_4/COS@β-CDOTs (**IV**), (e) Fe_3O_4/COS@β-CD-SO_3H NPs (**V**), and (f) Fe_3O_4/COS@β-CD-SO_3H NPs (**V**) after eight reuses

The characteristic band of β-CD is evident in the region of 1220–870 cm^{-1}, being due to asymmetric glycosidic C–O–C vibration. These results confirm successful grafting of β-CDOTs (**III**) onto the surface of Fe_3O_4/COS NPs (**II**) (Fig. 1d). Absorption bands at 1220–1190 and 1070–1020 cm^{-1} are related to both asymmetric and symmetric stretching vibration modes of O=S=O group. N–H bending and stretching vibrations appeared at 1660–1530 and 3450–3280 cm^{-1}, respectively (Fig. 1e). These results clearly confirm successful immobilization of taurine molecules on the surface of Fe_3O_4/COS@β-CDOTs (**IV**) (Fig. 1e).

Also, XRD analysis was applied to evaluate the crystallinity of the COS NPs and Fe_3O_4/COS NPs. Figure 2 shows the characteristic peaks at 2θ of 30.5°, 38.1°, 52.6°, 63.2°, 66.9°, and 79.1° corresponding to (1 1 1), (2 0 0), (2 2 0), (3 1 1), (2 2 2), and (4 0 0) crystallographic planes, in agreement with the standard data for CaO in Joint Committee on Powder Diffraction Standards (JCPDS) card no. 04-007-9734 [76]. The XRD results also demonstrate the presence of cubic CaO phase with high crystallinity. Moreover, in comparison with the COS NPs (**I**), diffraction peaks appeared at $2\theta = 29.4°$, 35.4°, 41.5°, 55.6°, 57.9°, and 62.1°, being associated with (2 2 0), (3 1 1), (4 0 0), (4 2 2), (5 1 1), and (4 4 0) reflections, in good accordance with the cubic phase of Fe_3O_4 MNPs (JCPDS 04-009-8428) [77]. The average crystallite size of the COS NPs (**I**) and Fe_3O_4/COS NPs (**II**) was calculated using the Debye–Scherrer equation $d = K\lambda/\beta\cos\theta$, yielding values of about 20 and 25 nm, respectively.

The morphology of the as-prepared nanostructured catalyst was studied using scanning electron microscopy (SEM). SEM images of Fe_3O_4/COS@β-CD-SO_3H NPs (**V**) (Fig. 3a, b) showed spherical morphology. Furthermore, energy-dispersive X-ray (EDX) spectroscopy confirmed the presence of Fe, Ca, Si, S, C, and O elements in the nanocatalyst structure, as shown in Fig. 4.

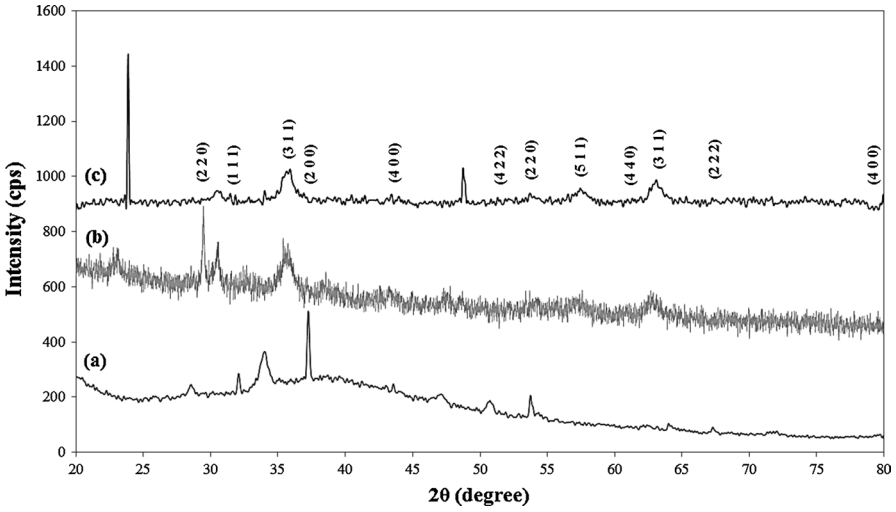

Fig. 2 XRD patterns of (a) COS NPs (**I**), (b) Fe_3O_4/COS NPs (**II**), and (c) Fe_3O_4/COS@β-CD-SO_3H NPs (**V**)

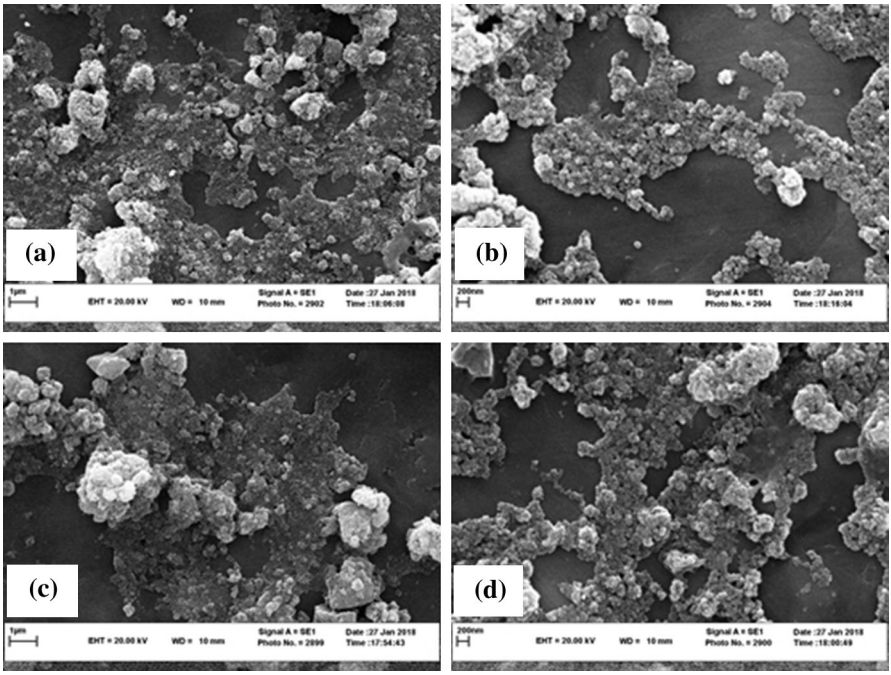

Fig. 3 SEM images of **a**, **b** Fe_3O_4/COS@β-CD-SO_3H NPs (**V**), and **c**, **d** Fe_3O_4/COS@β-CD-SO_3H NPs (**V**) after eight reuses

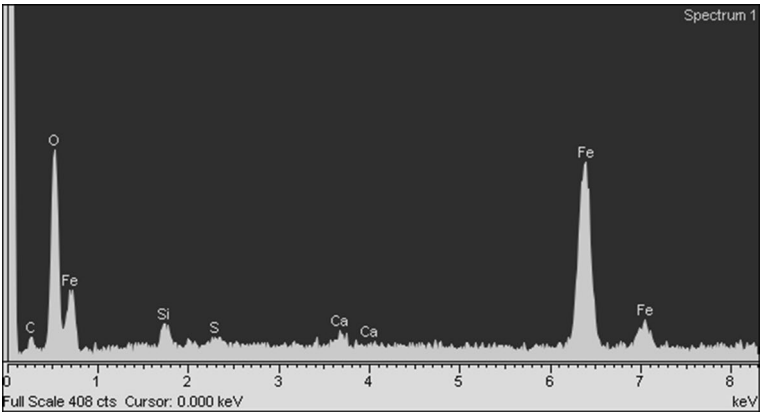

Fig. 4 EDX analysis of Fe_3O_4/COS@β-CD-SO_3H NPs (**V**)

The size and morphology of the Fe_3O_4/COS NPs (**II**) and Fe_3O_4/COS@β-CD-SO_3H NPs (**V**) were further characterized by transmission electron microscopy (TEM). As shown in Fig. 5, most of the particles displayed uniform spherical morphology with average particle size of about 20–50 nm, in good agreement with the values deduced from the XRD results. It can be seen that β-CDOTs (**III**) were

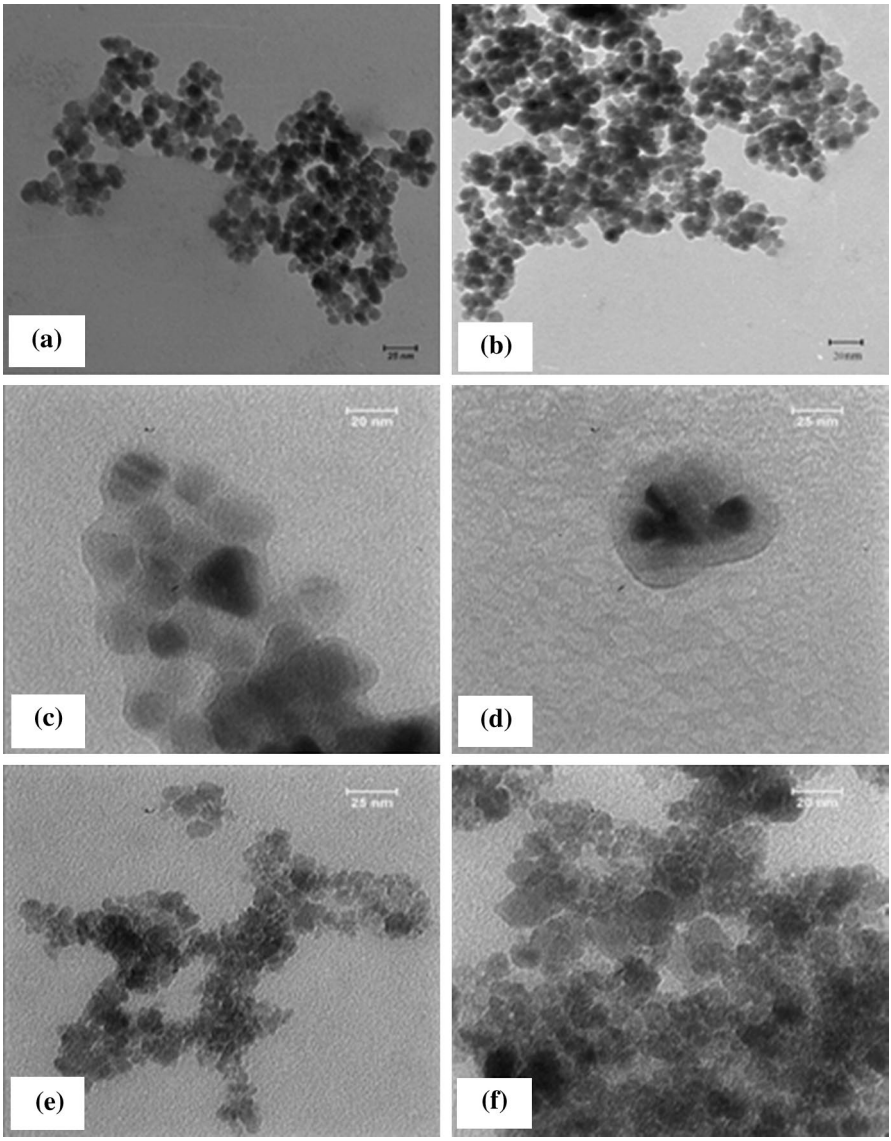

Fig. 5 TEM images of **a**, **b** Fe_3O_4/COS NPs (**II**), **c**, **d** Fe_3O_4/COS@β-CD-SO_3H NPs (**V**), and **e**, **f** Fe_3O_4/COS@β-CD-SO_3H NPs (**V**) after eight reuses

successfully immobilized on the surface of Fe_3O_4/COS NPs (**II**) through the reaction between Fe_3O_4/COS NPs (**II**) and –OH groups of the β-CDOTs (**III**) molecules (Fig. 5b, c).

The magnetization curves of the Fe_3O_4/COS NPs (**II**) and Fe_3O_4/COS@β-CD-SO_3H NPs (**V**), which are critical for this application, were measured at ambient temperature by vibrating-sample magnetometry (VSM). As illustrated in Fig. 6,

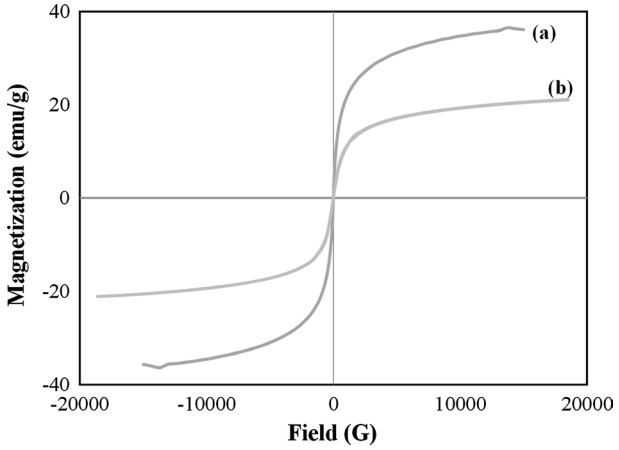

Fig. 6 Magnetization curves of (a) Fe_3O_4/COS NPs (**II**) and (b) Fe_3O_4/COS@β-CD-SO_3H NPs (**V**)

the saturation magnetization values of the Fe_3O_4/COS core–shell (**II**) and Fe_3O_4/COS@β-CD-SO_3H NPs (**V**) were 35.9 and 20.8 emu g^{-1}, respectively, being lower than the reference value for pure Fe_3O_4 MNPs [41]. This can be ascribed to communication at the interfaces between the COS NPs and Fe_3O_4 NPs in the composite [78]. However, the decline in the saturation magnetization of the Fe_3O_4/COS@β-CD-SO_3H NPs (**V**) can be attributed to the presence of the organic component (β-CD-SO_3H) functionalizing the surface of the Fe_3O_4/COS core–shell structures(**II**). Moreover, it is clearly seen from this figure that no remanence or coercivity were observed, indicating that the nanoparticles obtained in this study were superparamagnetic.

The thermal stability and amount of organic segment grafted onto the surface of Fe_3O_4/COS NPs were estimated by TGA/DTG of Fe_3O_4/COS@β-CD-SO_3H NPs (**V**). As shown in Fig. 7, the TGA thermogram of the nanocatalyst showed a ~ 2.0% weight loss at temperature near 100 °C, which is due to loss of residual water from the sample. Further, the next weight loss of ~ 20% from 150 to 630 °C is related to decomposition of β-CD-SO_3H groups on the surface of Fe_3O_4/COS NPs (**II**). This high temperature for β-CD-SO_3H elimination indicates the high thermal stability of Fe_3O_4/COS@β-CD-SO_3H NPs (**V**). According to the results obtained from TGA, the amount of organic component supported on the surface of Fe_3O_4/COS NPs (**II**) was estimated to be ~ 3.22 mmol g^{-1}. This result is also in good agreement with the elemental analysis results, showing carbon, nitrogen, and sulfur content of C = 35.86%, N = 4.48%, and S = 10.28%.

Furthermore, backtitration was used to determine the amount of carboxyl groups (acidic sites) on the Fe_3O_4/COS@β-CD-SO_3H NPs (**V**). To this purpose, a certain amount (100 mg) of nanoparticles was first reacted with NaOH solution (15 mL, 0.1 N), and the resulting mixture was maintained at room temperature for 24 h. Finally, the suspension was filtered and neutralized using standard HCl solution (0.1 M). According to the volume of HCl consumed (14.1 mL), the number of acidic sites was found to be 3.20 mmol g^{-1}.

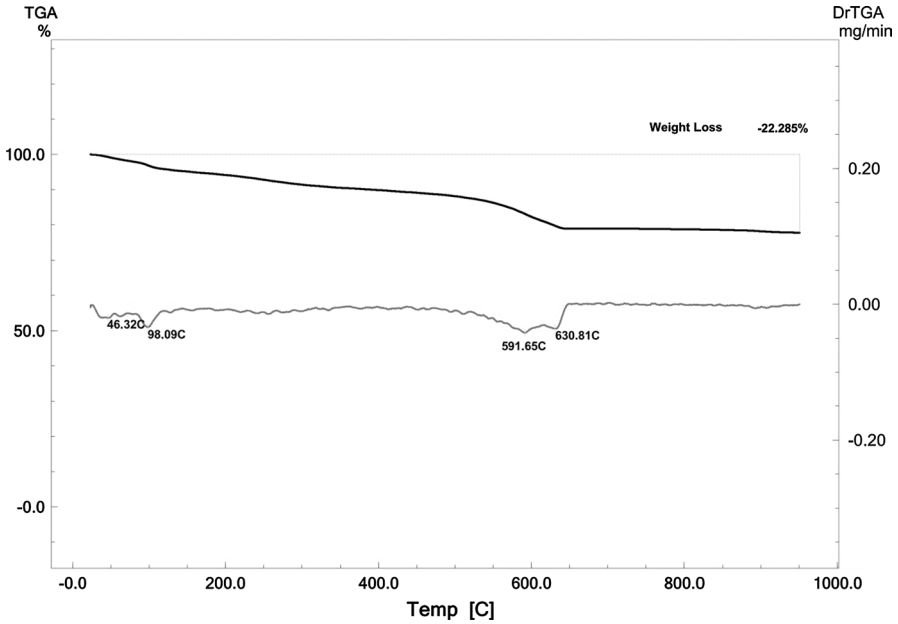

Fig. 7 TGA/DTG thermogram of Fe_3O_4/COS@β-CD-SO_3H NPs (**V**)

The results of elemental analysis of β-CDOTs (**III**) and the Fe_3O_4/COS@β-CD-SO_3H NPs (**V**) are presented in Table 1, showing good agreement with the TGA results and the calculation of the amount of acidic sites on the Fe_3O_4/COS@β-CD-SO_3H NPs (**V**).

Catalytic synthesis of spirooxindole derivatives

In our initial study, the merit of Fe_3O_4/COS@β-CD-SO_3H NPs (**V**) (as a heterogeneous acidic nanocatalyst) was investigated in the preparation of 2-amino-7,7-dimethyl-2′,5-dioxo-5,6,7,8-tetrahydrospiro[chromene-4,3′-indoline]-3-carbonitrile via one-pot multicomponent reaction of isatin (1 mmol), malononitrile (1 mmol), and dimedone (1 mmol) as model reaction under different conditions. The results are presented in Table 2. During our optimization studies, it was observed that, when the reaction was carried out without

Table 1 CHNS analysis results for β-CDOTs and Fe_3O_4/COS@β-CD-SO_3H NPs (**V**)

	β-CDOTs (**III**)				Fe_3O_4/COS@β-CD-SO_3H NPs (**V**)			
	C	H	N	S	C	H	N	S
w_i (calc.)/mass%	49.36	5.10	–	10.14	35.92	6.54	4.51	10.33
w_i (found)/mass%	49.22	5.04	–	10.09	35.86	6.51	4.48	10.28

Table 2 Optimization of various reaction parameters for synthesis of 2-amino-7,7-dimethyl-2′,5-dioxo-5,6,7,8-tetrahydrospiro[chromene-4,3′-indoline]-3-carbonitrile in presence of Fe_3O_4/COS@β-CD-SO_3H NPs (**V**)

Entry	Catalyst	Catalyst (g)	Solvent	Temperature (°C)	Time (min)	Isolated yield (%)
1	–	–	H_2O	50	18 h	Trace
2	Fe_3O_4 NPs	0.025	H_2O	50	18 h	10
3	COS NPs	0.025	H_2O	50	18 h	15
4	Fe_3O_4/COS NPs	0.025	H_2O	50	18 h	20
5	β-CD	0.025	H_2O	50	18 h	20
6	Fe_3O_4/COS@β-CDOTs NPs	0.025	H_2O	50	18 h	30
7	Taurine	0.025	H_2O	50	45	95
8	Fe_3O_4/COS@β-CD-SO_3H NPs	0.025	H_2O	50	20	98
9	Fe_3O_4/COS@β-CD-SO_3H NPs	0.025	H_2O	40	25	95
10	Fe_3O_4/COS@β-CD-SO_3H NPs	0.025	H_2O	60	20	98
11	Fe_3O_4/COS@β-CD-SO_3H NPs	0.020	H_2O	50	20	98
12	Fe_3O_4/COS@β-CD-SO_3H NPs	0.015	H_2O	50	35	90
13	Fe_3O_4/COS@β-CD-SO_3H NPs	0.020	EtOH	50	20	90
14	Fe_3O_4/COS@β-CD-SO_3H NPs	0.020	–	50	18 h	60

catalyst in water at 50 °C, the reaction was incomplete even after 18 h with a trace amount of the desired product obtained (Table 2, entry 1). To emphasize the essential role of Fe_3O_4/COS@β-CD-SO_3H NPs (**V**) in the preparation of spirooxindoles, in a set of experiments, the model reaction was conducted in presence of Fe_3O_4 NPs, COS NPs (**I**), Fe_3O_4/COS NPs (**II**), β-CD, and Fe_3O_4/COS@β-CD NPs (**III**) (Table 2, entries 2–6). In all cases, rather poor yield of product was obtained. To our delight, use of taurine and Fe_3O_4/COS@β-CD-SO_3H NPs (**V**) increased the yield significantly with shorter reaction time (Table 2, entries 7, 8). This is presumed to occur due to the acidity of taurine and Fe_3O_4/COS@β-CD-SO_3H NPs (**V**), which promotes the reaction effectively. The heterogeneity and magnetic reusability of Fe_3O_4/COS@β-CD-SO_3H NPs (**V**) as a green and solid acidic catalyst make it the best choice for catalytic preparation of spirooxindole derivatives. Decreasing the reaction temperature to 40 °C prolonged the reaction time to obtain the same yield (Table 2, entry 9), whereas an increase in the reaction temperature did not lead to any improvement in the yield of the product (Table 2, entry 10). Several sets of reactions were performed in presence of different amounts of catalyst (Table 2, entries 11, 12). Gratifyingly,

the desired product was produced in high yield when applying 0.020 g catalyst. To search for the best solvent system for the model reaction, the feasibility of the model reaction was examined in EtOH, and also under solvent-free conditions (Table 2, entries 13, 14). Interestingly, the results clearly revealed that the catalyst showed better activity in H_2O (98%, 20 min) or EtOH (90%, 20 min) compared with solvent-free conditions (60%, 18 h). Water and ethanol produced almost the same results, but based on environmental awareness, cost-effectiveness, and easy accessibility, we chose water as the solvent.

Having obtained the optimized condition, we delineated the versatility of the present methodology towards various substrates for synthesis of a series of desired spirooxindole products through the reaction of variously substituted isatins, different nitrilo active methylene components (malononitrile or ethyl cyanoacetate), and 1,3-dicarbonyl compounds. The results of this detailed study are presented in Table 3. The reactions proceeded rapidly, and the desired spirooxindoles with fused

Table 3 Synthesis of different structurally spirooxindoles in presence of Fe_3O_4/COS@β-CD-SO_3H NPs (**V**)

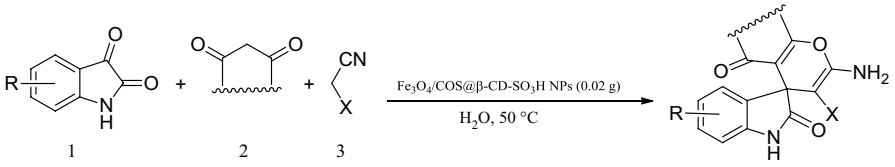

Entry	R	C–H activated	X	Product	Time (min)	Isolated yield (%)
1	H	Dimedone	CN	**4a**	20	98
2	5-Me	Dimedone	CN	**4b**	15	95
3	5-OMe	Dimedone	CN	**4c**	20	96
4	5-Cl	Dimedone	CN	**4d**	15	98
5	H	Dimedone	CO_2Et	**4e**	20	95
6	5-Me	Dimedone	CO_2Et	**4f**	22	94
7	5-OMe	Dimedone	CO_2Et	**4g**	20	95
8	5-Cl	Dimedone	CO_2Et	**4h**	20	94
9	H	Cyclohexane-1,3-dione	CN	**4i**	20	96
10	5-Me	Cyclohexane-1,3-dione	CN	**4j**	20	95
11	5-OMe	Cyclohexane-1,3-dione	CN	**4k**	20	96
12	5-Cl	Cyclohexane-1,3-dione	CN	**4l**	16	98
13	H	Cyclohexane-1,3-dione	CO_2Et	**4m**	20	94
14	5-Me	Cyclohexane-1,3-dione	CO_2Et	**4n**	20	96
15	5-OMe	Cyclohexane-1,3-dione	CO_2Et	**4o**	20	95
16	5-Cl	Cyclohexane-1,3-dione	CO_2Et	**4p**	15	96

tetrahydrochromene derivatives were obtained from a diverse set of reactants in high yield. The corresponding spirooxindoles (**4a**–**p**) were produced after 15–22 min by one-pot condensation reaction of various isatins (bearing electron-donating groups as well as electron-withdrawing substituent) with malononitrile or ethyl cyanoacetate, and dimedone or cyclohexane-1,3-dione.

Likewise, after longer reaction times, trace amounts of desired products were produced when using isatins substituted at 4- and 7-position with malononitrile or ethyl cyanoacetate, and dimedone or cyclohexane-1,3-dione.

All products were crystalline and fully characterized based on their melting point and mass spectrometry. Additionally, the structures of selected compounds (**4a**, **b**, **c**, **e**, **g**, **m**, **o**) were further recognized by FT-IR and ^{1}H and ^{13}C nuclear magnetic resonance (NMR) spectroscopy. The common spectral features of all these compounds are the presence of cyano and amino groups in the FT-IR spectra; the stretching frequency appeared in the range of 2200–2190 cm^{-1}, corroborating the presence of –CN group, while the stretching frequency in the range of 3377–3140 cm^{-1} corresponds to $–NH_2$ functional group. In the ^{1}H NMR spectra, a broad singlet resonating in the range of 10.5–10 ppm established the $–NH_2$ at 11-position. Besides, in ^{13}C NMR spectra, a characteristic peak at around 110–108 ppm verified the carbon of cyano group.

According to the above results, the following possible mechanism can be proposed to account for the formation of spirooxindole derivatives in presence of Fe_3O_4/COS@β-CD-SO_3H NPs (**V**) via a typical cascade reaction (Scheme 3): Owing to their acidic nature, Fe_3O_4/COS@β-CD-SO_3H NPs (**V**) might serve as a Brønsted-acid catalyst in several stages and play a crucial role in accelerating the condensation of isatin with nitrilo active methylene components (malononitrile or ethyl cyanoacetate) to afford **I** (see Table 2, entry 1). In the subsequent step, the electron-deficient adduct **I** is attacked through acid-promoted Michael addition of activated 1,3-dicarbonyl compound to give intermediate **II**. Further intramolecular cyclization furnishes the desired product **III**. Previous literature reports also support this proposed mechanism [79].

From the viewpoint of green chemistry, recyclability is an essential aspect for a good and efficient catalyst. In this regard and to show an additional advantage of our developed catalytic system, the reusability of Fe_3O_4/COS@β-CD-SO_3H NPs (**V**) was studied in the model reaction under the optimized reaction conditions (Table 2, entry 11). After reaction completion, the magnetic nanocatalyst was easily separated using the simple means of a external magnet, washed with EtOH and then H_2O to remove all organic compounds, then dried at 50 °C for 24 h. Then, the nanocatalyst was reused for the next batch under the same experimental condition and recycled again. It is interesting to note that almost equal efficiency as when using the fresh nanocatalyst was obtained when using the recovered catalyst up to eight times (Fig. 8). These results evidently demonstrate that the initial catalytic activity of the present magnetic nanocatalyst was substantially retained even after repeated applications.

After completion of eight cycles, we analyzed the magnetic nanocatalyst using FT-IR spectroscopy, XRD analysis, SEM, and TEM. The FT-IR spectrum of the Fe_3O_4/COS@β-CD-SO_3H NPs (**V**) after eight reuses (Fig. 1f) illustrated

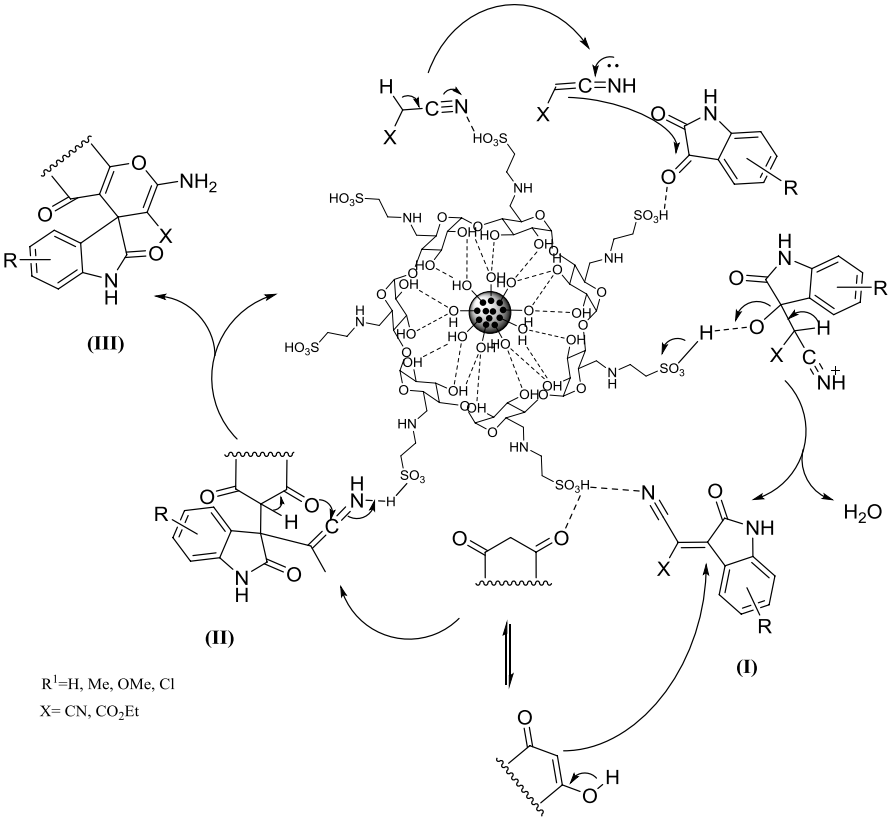

Scheme 3 Proposed mechanism for synthesis of spirooxindoles using Fe_3O_4/COS@β-CD-SO_3H NPs (**V**)

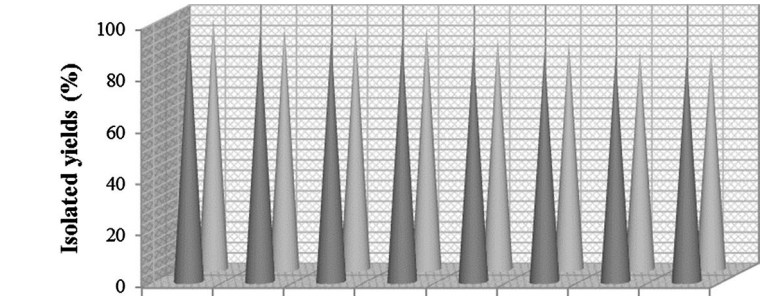

Fig. 8 Synthesis of 2-amino-7,7-dimethyl-2′,5-dioxo-5,6,7,8-tetrahydrospiro[chromene-4,3′-indoline]-3-carbonitrile in presence of reused Fe_3O_4/COS@β-CD-SO_3H NPs (**V**)

that no substantial changes occurred in the chemical structure of the catalyst. All the characteristic absorption bands of functional groups and hydrogen-bonding network of the nanocatalyst after uses were well preserved in terms of shape, position, and relative intensity. Moreover, the XRD results (Fig. 2c) and SEM (Fig. 3c, d) and TEM images (Fig. 5e, f) of the nanostructured catalyst after right reuses clearly indicated that no significant changes (no significant changes or shifts in the characteristic XRD peaks; no changes in morphology, shape, or size in SEM and TEM images) occurred in the chemical structure of the catalyst after eight runs.

Backtitration of the Fe_3O_4/COS@β-CD-SO_3H NPs (**V**) after right reuses revealed that the amount of $NHCH_2CH_2SO_3H$ loaded per 1.000 g of nanocatalyst decreased to 3.15 mmol. This result clearly indicates that 5% (a negligible amount) of the active acidic sites had leached out from the surface of the catalyst after eight reaction runs (fresh catalyst contained 3.2 mmol –$NHCH_2CH_2SO_3H$ per 1.000 g).

The catalytic ability of Fe_3O_4/COS@β-CD-SO_3H NPs (**V**) in one-pot multicomponent preparation of 2-amino-7,7-dimethyl-2′,5-dioxo-5,6,7,8-tetrahydrospiro[chromene-4,3′-indoline]-3-carbonitrile is compared with catalysts previously reported in literature in Table 4. Although other catalysts can afford high yield of the product, some of these methods suffer from one or more disadvantages, such as long reaction time (entries 1–5, 7–11), high catalyst loading (entries 1–11), corrosive reagent (entry 3), tedious workup procedures and catalyst nonreusability (entries 1–6).

Conclusions

Fe_3O_4/COS@β-CD-SO_3H NPs (**V**) were prepared as a new environmentally friendly magnetic nanostructured catalyst. The as-prepared green solid-phase acidic nanocatalyst was well characterized by various techniques such as FT-IR spectroscopy, XRD analysis, SEM, EDX spectroscopy, TEM, VSM, TGA, and elemental analysis and evaluated in one-pot three-component synthesis of spirooxindoles with fused chromenes in green solvent (H_2O). The characterization results revealed uniform spherical morphology with average particle size of about 16–25 nm and confirmed the superparamagnetic behavior of the Fe_3O_4/COS@β-CD-SO_3H NPs (**V**). Fe_3O_4/COS@β-CD-SO_3H NPs (**V**) is highlighted as a better catalyst in terms of product yield, mild reaction condition, reaction time, use of H_2O as green reaction medium, and simple experimental and isolation procedures. The magnetic acidic catalyst was prepared simply, removed from the reaction mixture using an external magnetic field, and reused eight times without appreciable loss of activity. Use of this catalyst is more cost-effective compared with recently reported catalysts. Due to the advantages of this protocol over previously reported methods, it can be expected that the present methodology will find extensive application in combinatorial chemistry as well as in multicomponent green synthesis to afford different types of spirooxindole fused heterocycles. Moreover, as this method does not involve use of hazardous organic solvents, it can be classified as a green chemistry approach.

Table 4 Comparison between efficiency of Fe_3O_4/COS@β-CD-SO_3H NPs (V) and some other catalysts for preparation of 2-amino-7,7-dimethyl-2′,5-dioxo-5,6,7,8-tetrahydrospiro[chromene-4,3′-indoline]-3-carbonitrile

Entry	Catalyst (mol%)	Solvent	Temperature (°C)	Time (min)	Yield (%)	Reusability (runs)	Ref.
1	Sodium stearate (10)	H_2O	60	180	95	–	[13]
2	$Cu(OAc)_2{\cdot}H_2O$ (20)	–	80	240	86	–	[17]
3	I_2 (10)	H_2O	50	60	80	–	[7]
4	TEBA[a] (20)	H_2O	60	180	90	–	[5]
5	Lipase (30 mg)	EtOH	30	180	94	–	[10]
6	Oxalic acid dihydrate: proline (LTTM) (5 ml)	–	R.T.	30	94	–	[11]
7	Nano-MgO (15)	H_2O	80	120	93	4	[19]
8	AHST-MNPs[b] (0.07 g)	H_2O	60	105	94	–	[24]
9	(SB-DBU)Cl[c] (5)	EtOH	R.T.	120	95	15	[25]
10	SSA-MNPs[d] (0.1 g)	EtOH-H_2O	60	80	95	–	[23]
11	Carbon–SO_3H (10)	EtOH	Reflux	180	81	5	[26]
12	Fe_3O_4/COS@β-CD-SO_3H NPs (0.018[e])	H_2O	50	20	98	8	Present study

[a]Triethylbenzylammonium chloride

[b]*S*-alkyl *O*-hydrogen sulfothioate-functionalized silica-coated magnetic nanoparticles

[c]Silica-bonded 5-*n*-propyl-octahydro-pyrimido[1,2-*a*]azepinium chloride

[d]Silica sulfuric acid magnetic nanoparticle

[e]mol% of –SO_3H groups

Experimental

General

All chemical reagents and solvents were purchased from Merck and Sigma-Aldrich chemical companies and used as received without further purification. Purity determinations of the products were accomplished by thin-layer chromatography (TLC) on silica gel Polygram SIL G/UV 254 plates. Melting points of products were determined using an Electrothermal type 9100 melting point apparatus. FT-IR spectra were obtained from pressed KBr pellets using an AVATAR 370 FT-IR spectrometer (Thermo Nicolet, USA) at room temperature in the range from 4000 and 400 cm^{-1} with resolution of 4 cm^{-1}. Elemental analysis was performed using a Thermo Finnigan Flash EA 1112 series instrument. NMR spectra were obtained using Bruker Avance 300 MHz instruments in dimethylsulfoxide (DMSO)-d_6. Mass spectra were recorded with a CH7A Varian MAT Bremen instrument at 70 eV electron impact ionization and are reported in *m*/*z* (rel %). The crystal structure of the catalyst was analyzed by XRD using a Bruker D8 Avance diffractometer operated at 40 kV and 30 mA with Cu K_α radiation ($\lambda = 0.154$ Å). SEM images were recorded using a Leo1450 VP scanning electron microscope at accelerating voltage of 20 kV. Elemental compositions were determined using an SC7620 energy-dispersive X-ray (EDX) instrument presenting 133 eV resolution at 20 kV. Transmission electron microscopy (TEM) was performed with a Leo 912 AB microscope (Zeiss, Germany) at accelerating voltage of 120 kV. TGA was carried out using a Shimadzu thermogravimetric analyzer (TG-50) in the temperature range of 25–900 °C at heating rate of 10 °C min^{-1} under air atmosphere. The magnetic properties of the catalyst were measured using a vibrating-sample magnetometer (VSM, 7400 Lake Shore). All products are known compounds and were characterized based on their FT-IR, ^{1}H NMR, and ^{13}C NMR, and mass spectra plus comparison of their melting points with known compounds. All yields refer to isolated products after purification by recrystallization.

Preparation of calcined oyster shells (I)

Oyster shells were washed several times with H_2O/EtOH to remove impurities, then dried for 12 h at 100 °C. The oyster shells were crushed and milled to obtain fine powder. Subsequently, calcined oyster shells (COS) were generated by calcination of waste oyster shells at high temperature (900 °C for 6 h).

Hydrothermal synthesis of Fe_3O_4/COS NPs (II)

A suspension of calcined oyster shell (COS) (2 g) in deionized water (150 mL) was added to a 500-mL three-necked flask. Then, $FeCl_3 \cdot 6H_2O$ (9.2 mmol, 2.48 g) and $FeCl_2 \cdot 4H_2O$ (4.6 mmol, 1.26 g) were added to the white suspension. The resulting mixture was mechanically stirred for 3 min at room temperature under Ar

atmosphere. Subsequently, ammonium hydroxide (20 mL, 25%) was dropped very slowly into the mixture under stirring. The resulting black mixture was stirred continuously for 5 h at 75 °C under Ar atmosphere. Finally, the mixture was permitted to cool to room temperature, and Fe_3O_4/COS MNPs were separated by an external magnet and washed with deionized water several times before being dried under vacuum at 50 °C overnight.

Preparation of tosylated β-cyclodextrin (β-CDOTs) (III)

To a suspension of β-CD (1 mmol, 1.134 g) in water (10 mL), NaOH (7 M, 2 mL) was added dropwise slowly. When the suspension turned to a homogeneous phase, the flask was immersed in an ice–water bath. Afterward, a solution of *p*-toluenesulfonyl chloride (10.5 mmol, 2 g) in acetonitrile (4 mL) was dripped into the clear solution over 20 min. After stirring for 3 h at ambient temperature, the remaining precipitate was refrigerated overnight at 4 °C. Subsequently, the white precipitate was removed by filtration and recrystallized from hot water to obtain a pure white solid (1.971 g, 89%).

Preparation of Fe_3O_4/COS@β-CDOTs NPs (IV)

Fe_3O_4/COS NPs (1 g) were dispersed in dry DMF by sonication for 20 min, then β-CDOTs (1.32 mmol, 1.5 g) was added to the suspension. The mixture was refluxed with vigorous stirring. After 24 h, the resulting Fe_3O_4/COS@β-CDOTs NPs were collected using an external magnet, washed with distilled water, then dried at 50 °C for 6 h.

Preparation of magnetic calcined oyster shell functionalized with taurine immobilized on β-cyclodextrin (Fe_3O_4/COS@β-CD-SO_3H NPs) (V)

Taurine (40.00 mmol, 5 g) was added to a suspension of Fe_3O_4/COS@β-CDOTs NPs (**V**) (1 g) in distilled water (80 mL) with stirring at 60 °C. After 24 h, the mixture was permitted to cool to room temperature. Thereafter, Fe_3O_4/COS@β-CD-SO_3H nanoparticles (**V**) were separated by an external magnet and washed with deionized water several times before being dried under vacuo at 50 °C overnight.

Typical procedure for preparation of 2-amino-7,7-dimethyl-2′,5-dioxo-5,6,7,8 -tetrahydrospiro[chromene-4,3′-indoline]-3-carbonitrile in presence of Fe_3O_4/COS@β-CD-SO_3H NPs (V)

Fe_3O_4/COS@β-CD-SO_3H NPs (**V**) (0.02 g) were added to a mixture of isatin (1 mmol, 0.147 g), 5,5-dimethylcyclohexane-1,3-dione (dimedone) (1 mmol, 0.140 g), and malononitrile (1 mmol, 0.066 g) in water (4 mL). The mixture was magnetically stirred at 50 °C, for 20 min. Reaction progress was monitored by TLC (*n*-hexane:EtOAc, 3:1). Upon reaction completion, the catalyst was removed by an external magnet, washed with water (10 mL), and dried overnight to be ready for the

next run. The formed solid was filtered off, washed with warm water, then dried to obtain pure products (0.328 g, 98%).

Acknowledgements The authors gratefully acknowledge partial support of this study by Ferdowsi University of Mashhad Research Council (Grant no. 3/43388).

References

1. K. Ding, Y. Lu, Z. Nikolovska-Coleska, G. Wang, S. Qiu, S. Shangary, W. Gao, D. Qin, J. Stuckey, K. Krajewski, P.P. Roller, S. Wang, J. Med. Chem. **49**, 3432 (2006)
2. C.V. Galliford, K.A. Scheidt, Angew. Chem. Int. Ed. **46**, 8748 (2007)
3. C. Konkoy, D. Fick, S. Cai, N. Lan, J. Keana, in *Chem. Abst.* (2001), p. 29313a
4. M. Zhang, Q.-Y. Fu, G. Gao, H.-Y. He, Y. Zhang, Y.-S. Wu, Z.-H. Zhang, ACS Sustain. Chem. Eng. **5**, 6175 (2017)
5. S.-L. Zhu, S.-J. Ji, Y. Zhang, Tetrahedron **63**, 9365 (2007)
6. Y.M. Litvinov, V.Y. Mortikov, A.M. Shestopalov, ACS Comb. Sci. **10**, 741 (2008)
7. M. Kidwai, A. Jain, V. Nemaysh, R. Kumar, P.M. Luthra, Med. Chem. Res. **22**, 2717 (2013)
8. S. Gao, C.H. Tsai, C. Tseng, C.-F. Yao, Tetrahedron **64**, 9143 (2008)
9. M. Dabiri, M. Bahramnejad, M. Baghbanzadeh, Tetrahedron **65**, 9443 (2009)
10. S.-J. Chai, Y.-F. Lai, J.-C. Xu, H. Zheng, Q. Zhu, P.-F. Zhang, Adv. Synth. Catal. **353**, 371 (2011)
11. D.R. Chandam, A.G. Mulik, D.R. Patil, M.B. Deshmukh, Res. Chem. Intermed. **42**, 1411 (2016)
12. A. Dandia, V. Parewa, A.K. Jain, K.S. Rathore, Green Chem. **13**, 2135 (2011)
13. L.-M. Wang, N. Jiao, J. Qiu, J.-J. Yu, J.-Q. Liu, F.-L. Guo, Y. Liu, Tetrahedron **66**, 339 (2010)
14. K. Rad-Moghadam, L. Youseftabar-Miri, Tetrahedron **67**, 5693 (2011)
15. B. Sadeghi, M. Ghasemi Pirbaluti, P. Farokhi Nezhad, R. Abbasi Nezhad, Res. Chem. Intermed. **41**, 4047 (2015)
16. G. Mohammadi Ziarani, A. Badiei, S. Mousavi, N. Lashgari, A. Shahbazi, Chin. J. Catal. **33**, 1832 (2012)
17. F. Mohamadpour, M.T. Maghsoodlou, R. Heydari, M. Lashkari, Res. Chem. Intermed. **42**, 7841 (2016)
18. C. Bodhak, A. Kundu, A. Pramanik, RSC Adv. **5**, 85202 (2015)
19. B. Karmakar, A. Nayak, J. Banerji, Tetrahedron Lett. **53**, 5004 (2012)
20. R.-Y. Guo, P. Wang, G.-D. Wang, L.-P. Mo, Z.-H. Zhang, Tetrahedron **69**, 2056 (2013)
21. M. Daraie, Y.S. Beheshtiha, M.M. Heravi, Monatsh. Chem. Chem. Mon. **146**, 191 (2015)
22. R. Ghahremanzadeh, Z. Rashid, A.H. Zarnani, H. Naeimi, Appl. Catal. A **467**, 270 (2013)
23. A.R. Karimi, M. Sourinia, Z. Dalirnasab, M. Karimi, Can. J. Chem. **93**, 546 (2015)
24. A.R. Karimi, R. Davood Abadi, Z. Dalirnasab, Res. Chem. Intermed. **41**, 7427 (2015)
25. A. Hasaninejad, N. Golzar, M. Beyrati, A. Zare, M.M. Doroodmand, J. Mol. Catal. A Chem. **372**, 137 (2013)
26. B. Maheshwar Rao, G.N. Reddy, T.V. Reddy, B.L.A.P. Devi, R.B.N. Prasad, J.S. Yadav, B.V.S. Reddy, Tetrahedron Lett. **54**, 2466 (2013)
27. A. Thakur, M. Tripathi, U.C. Rajesh, D.S. Rawat, RSC Adv. **3**, 18142 (2013)
28. S.P. Satasia, P.N. Kalaria, J.R. Avalani, D.K. Raval, Tetrahedron **70**, 5763 (2014)
29. S.S.E. Ghodsinia, B. Akhlaghinia, RSC Adv. **5**, 49849 (2015)
30. S.S.E. Ghodsinia, B. Akhlaghinia, R. Jahanshahi, RSC Adv. **6**, 63613 (2016)
31. R. Jahanshahi, B. Akhlaghinia, RSC Adv. **5**, 104087 (2015)
32. R. Jahanshahi, B. Akhlaghinia, RSC Adv. **6**, 29210 (2016)
33. E. Karimian, B. Akhlaghinia, S.S.E. Ghodsinia, J. Chem. Sci. **128**, 429 (2016)
34. S.M. Masjed, B. Akhlaghinia, M. Zarghani, N. Razavi, Aust. J. Chem. **70**, 33 (2017)
35. N. Mohammadian, B. Akhlaghinia, Res. Chem. Intermed. **43**, 22 (2017)
36. N. Razavi, B. Akhlaghinia, RSC Adv. **5**, 12372 (2015)
37. N. Razavi, B. Akhlaghinia, New J. Chem. **40**, 447 (2016)
38. N.Y. Siavashi, B. Akhlaghinia, M. Zarghani, Res. Chem. Intermed. **42**, 5789 (2016)
39. Z. Zarei, B. Akhlaghinia, Chem. Pap. **69**, 1421 (2015)
40. Z. Zarei, B. Akhlaghinia, RSC Adv. **6**, 106473 (2016)

41. M. Zarghani, B. Akhlaghinia, Appl. Organomet. Chem. **29**, 683 (2015)
42. M. Zarghani, B. Akhlaghinia, RSC Adv. **5**, 87769 (2015)
43. M. Zarghani, B. Akhlaghinia, RSC Adv. **6**, 31850 (2016)
44. M. Zarghani, B. Akhlaghinia, RSC Adv. **6**, 38592 (2016)
45. M. Zarghani, B. Akhlaghinia, Bull. Chem. Soc. Jpn. **89**, 1192 (2016)
46. R. Jahanshahi, B. Akhlaghinia, Chem. Pap. **71**, 1351 (2017)
47. S.S.E. Ghodsinia, B. Akhlaghinia, Green Chem. (2019). https://doi.org/10.1039/C8GC03931C
48. M.S. Ghasemzadeh, B. Akhlaghinia, New J. Chem. **43**, 5341 (2019)
49. S. Pakdel Asgarabad, B, Akhlaghinia, A. Mohammadinezhad, Chem. Africa 1 (2019)
50. H. Karimzadegan, B. Akhlaghinia, M.S. Ghasemzadeh, Iran. J. Catal. (2019) (**in press)**
51. M. Zamani, B. Akhlaghinia, A. Mohammadinezhad, ChemistrySelect **3**, 9431 (2018)
52. B. Akhlaghinia, P. Sanati, A. Mohammadinezhad, Z. Zareie, Res. Chem. Intermed. **45**, 3215 (2019)
53. A. Mohammadinezhad, B. Akhlaghinia, Green Chem. **19**, 5625 (2017)
54. Z. Zarei, B. Akhlaghinia, New J. Chem. **41**, 15485 (2017)
55. R. Jahanshahi, B. Akhlaghinia, New J. Chem. **41**, 7203 (2017)
56. N. Mohammadian, B. Akhlaghinia, Res. Chem. Intermed. **44**, 18 (2018)
57. R. Jahanshahi, B. Akhlaghinia, Res. Chem. Intermed. **44**, 2451 (2018)
58. M. Nejatianfar, B. Akhlaghinia, R. Jahanshahi, Appl. Organomet. Chem. **32**, 4095 (2018)
59. A. Mohammadinezhad, B. Akhlaghinia, Aust. J. Chem. **71**, 32 (2017)
60. A. Schätz, M. Hager, O. Reiser, Adv. Funct. Mater. **19**, 2109 (2009)
61. M. Zhang, Y.-H. Liu, Z.-R. Shang, H.-C. Hu, Z.-H. Zhang, Catal. Commun. **88**, 39 (2017)
62. M.-N. Chen, L.-P. Mo, Z.-S. Cui, Z.-H. Zhang, Curr. Opin. Green Sustain. Chem. **15**, 27 (2019)
63. M. Zhang, P. Liu, Y.-H. Liu, Z.-R. Shang, H.-C. Hu, Z.-H. Zhang, RSC Adv. **6**, 106160 (2016)
64. S. Sobhani, R. Jahanshahi, New J. Chem. **37**, 1009 (2013)
65. Q. Li, G. Tang, X. Xiong, Y. Cao, L. Chen, F. Xu, H. Tan, Sens. Actuators B Chem. **215**, 86 (2015)
66. M. Arana, S.E. Jacobo, H. Troiani, P.G. Bercoff, IEEE Trans. Magn. **49**, 4547 (2013)
67. B. Tural, N. Özkan, M. Volkan, J. Phys. Chem. Solids **70**, 860 (2009)
68. A.P. Herrera, M. Rodriguez, M. Torres-Lugo, C. Rinaldi, J. Mater. Chem. **18**, 855 (2008)
69. Z. Durmus, H. Kavas, M.S. Toprak, A. Baykal, T.G. Altınçekiç, A. Aslan, A. Bozkurt, S. Coşgun, J. Alloys Compd. **484**, 371 (2009)
70. H. Wei, N. Insin, J. Lee, H.-S. Han, J.M. Cordero, W. Liu, M.G. Bawendi, Nano Lett. **12**, 22 (2012)
71. M.A. Nasseri, F. Kamali, B. Zakerinasab, RSC Adv. **5**, 26517 (2015)
72. H.R. Safaei, M. Shekouhy, S. Rahmanpur, A. Shirinfeshan, Green Chem. **14**, 1696 (2012)
73. J. Zhou, Z. Dong, H. Yang, Z. Shi, X. Zhou, R. Li, Appl. Surf. Sci. **279**, 360 (2013)
74. M. Osada, C. Miura, Y.S. Nakagawa, M. Kaihara, M. Nikaido, K. Totani, Carbohydr. Polym. **92**, 1573 (2013)
75. F.G. Pearson, R.H. Marchessault, C.Y. Liang, J. Polym. Sci. **43**, 101 (1960)
76. G. Vidal-Valat, J.P. Vidal, K. Kurki-Suonio, Acta Crystallogr. A **34**, 594 (1978)
77. H. Okudera, K. Kihara, T. Matsumoto, Acta Crystallogr. B **52**, 450 (1996)
78. G.H. Du, Z.L. Liu, X. Xia, Q. Chu, S.M. Zhang, J. Sol-Gel. Sci. Technol. **39**, 285 (2006)
79. A. Khalafi-Nezhad, S. Mohammadi, ACS Comb. Sci. **15**, 512 (2013)